Cadmium isotope fractionation during complexation with humic acid

Gildas Ratié, Vladislav Chrastny, Damien Guinoiseau, Remi Marsac, Zuzana Vaňková, Michael Komárek

Cadmium isotope fractionation during complexation with humic acid

Gildas Ratié[1], Vladislav Chrastný[1], Damien Guinoiseau[2,3], Rémi Marsac[4], Zuzana Vaňková[1], Michael Komárek[1*]

[1] Department of Environmental Geosciences, Faculty of Environmental Sciences, Czech University of Life Sciences Prague, Kamýcká 129, 165 00, Prague – Suchdol, Czech Republic

[2]Université de Paris, Institut de physique du globe de Paris, CNRS, F-75005 Paris, France

[3] Aix Marseille Univ, CNRS, IRD, INRAE, Coll France, CEREGE, Aix-en-Provence, France.

[4] Univ Rennes, CNRS, Géosciences Rennes - UMR 6118, F-35000 Rennes, France

*corresponding author: komarek@fzp.czu.cz

Keywords

cadmium isotopes; humic acid; carboxylic groups; non-specific binding; electrostatic attractions; cadmium hydration complexes

Abstract

Cadmium (Cd) isotopes are known to fractionate during complexation with various environmentally relevant surfaces and ligands. Our results, which were obtained using a combination of various techniques and approaches, highlight the preferential enrichment of light Cd isotopes bound to humic acid (HA), leaving preferentially the heavier Cd pool in the solution ($\Delta^{114/110}Cd_{HA\text{-}Cd(aq)}$ of -0.15 ± 0.01‰). At high ionic strengths, Cd isotope fractionation mainly depends on its complexation with carboxylic sites. Outer-sphere complexation occurs at equilibrium together with inner-sphere complexation as well as with the change of the first Cd coordination and its hydration complexes in solution. At low ionic strengths, non-specific Cd binding induced by electrostatic attractions plays a dominant role and promotes Cd isotope fractionation during complexation. This significant outcome

elucidates the mechanisms involved in HA-Cd interactions. The results can be used during (i) fingerprinting the available Cd in soil solution after its complexation with solid or soluble natural organic matter and (ii) evaluate the contribution of Cd complexation with organic ligands and phytoplankton-derived debris *vs.* Cd assimilation by phytoplankton in seawater.

1. Introduction

Besides other "non-traditional" isotopes that have been studied increasingly during the last couple of decades, Cd has drawn much interest as the knowledge of Cd isotope systematics is crucial for a thorough understanding of the Earth's Cd geochemistry cycle. Pilot studies involving Cd isotopes date back to the 1970s, when large variations were measured in meteoritic and extraterrestrial materials.[1,2] Cadmium has six stable isotopes (^{106}Cd, ^{108}Cd, ^{110}Cd, ^{111}Cd, ^{112}Cd, ^{114}Cd) and its isotope systematics can be used in different fields: (i) marine biogeochemistry and oceanography, given the nutrient-like behavior of Cd and its close correlation with algal nutrients, e.g., nitrate and phosphate,[3–6] (ii) Cd plant uptake in the soil-plant system influenced by the applications of mineral P fertilizers containing Cd and the risk of Cd transfer into the food chain,[7–11] and (iii) natural and anthropogenic source tracking based on the large isotope fractionation induced by evaporation and condensation processes during industrial Cd emissions.[12–15]

Despite these numerous environmental studies, there is a surprising lack of a fundamental understanding of Cd isotope fractionation at specific conditions. Bioavailability, mobility, and toxicity of Cd depend on its speciation in the natural system. Cadmium does not undergo natural redox reactions in such natural settings, so the most likely processes affecting its mobility are precipitation and adsorption/complexation with mineral or organic particles. Only four laboratory experiments have been conducted to quantify Cd isotope fractionation during adsorption[16] and (co)precipitation.[17–19] The results showed that lighter Cd isotopes are preferentially adsorbed to Mn-oxyhydroxides[16] ($\Delta^{114/110}Cd_{solid\text{-}Cd(aq)}$ = -0.54 to -0.24 ‰) and precipitated to calcite[17] ($\Delta^{114/110}Cd_{CaCO3\text{-}Cd(aq)} \approx$ -0.45‰) or as CdS[18] (closed-system Rayleigh fractionation model $1.00028 < \alpha_{Cd(aq)\text{-}CdS} < 1.00052$ for ^{114}Cd/^{110}Cd).

The mobility of Cd and its inherent toxicity to living organisms and humans[20–22] has motivated the scientific community to understand its sources and behavior in the environment.[23] By the end of the 1980s, Cd mobilization from anthropogenic sources (mining, metal smelting, manufacturing, and fertilizer use) was more than 5,000 times higher than from natural weathering.[24] Therefore, significant Cd amounts were remobilized in the biosphere resulting in an enrichment in the atmosphere, soils, sediments, and aquatic environments relative to its concentration in the continental crust.[25,26] Organo-Cd complexes are usually the primary chemical Cd species at different biogeochemical interfaces, i.e., soil-plants, sediment-surface waters-ocean, and strongly influence its behavior and fate in the environment.[10,27,28] The principal components of natural organic matter (NOM) are humic substances, i.e., fulvic acids, humin, and humic acids (HA), the latter being a heterogeneous high-molecular-weight organic material, which is ubiquitous in terrestrial (soil, peat) and aquatic environments (sediment, ocean, and freshwater), in both soluble and insoluble forms.[29–31] The physical, chemical, and microbiological transformations of plant, animal, algal, and microbial material[32] lead to the formation of HA through different humification processes,[30] generating variable and complex organic molecules. Humic acids are an important source of dissolved complexing organic ligands, such as carboxylic and phenolic hydroxyl groups[33] and these complexes affect the speciation of metal ions, together with their bioavailability, mobility, and toxicity.[34–37] Therefore, Cd complexation by HA is a crucial process influencing the biogeochemical cycling of Cd in the ocean, in the soil-plant system, or in general, during its remobilization in the environment.

The first objective of this study is to examine Cd complexation with a commonly used representative HA, i.e., leonardite humic acid, at different experimental conditions (Cd concentration, ionic strength, pH). The second objective is to determine the Cd isotope fractionation occurring during Cd complexation with HA under the same experimental conditions by measuring both dissolved (aqueous Cd) and complexed (Cd bound to HA) phases. Finally, combining Fourier transformation infrared (FTIR), X-ray absorption spectroscopy (XAS), and modeling, our study highlights the complexation mechanisms leading to Cd isotope fractionation during its complexation with HA.

2. Materials and Methods

2.1. Sorption experiments

2.1.1. Leonardite humic acid

Leonardite (humic acid) was chosen due to its high potential for complexation of metal(loid)s in aqueous solutions (As, Cd, Cu, Pb, Ni, etc.) and because it is commonly used as a NOM proxy.[38–40] Leonardite is a coal-like substance and is believed to be derived from lignitic coal *via* natural oxidation.[41] Leonardite has a greater oxygen content than lignite due to a larger number of carboxylic groups. Leonardite is composed of phenolic and carboxylic OH groups, aliphatic CH groups, and carbonyl groups together with conjugated carbonyl or aromatic groups[41]. In this study, leonardite HA was obtained from the International Humic Substances Society (IHSS) (C = 63.8%, O = 31.3%, H = 3.70% and N = 1.23%, HA/DOC = 1.57) and characterized by infrared spectroscopy (Fig. S1). For Fourier transform infrared spectroscopy (FTIR) analysis, samples were grounded with KBr at a 1/100 mass ratio and then pressed into disks. FTIR spectra were recorded using a FTIR spectrometer (Perkin Elmer) between 5000 and 400 cm^{-1} at a resolution of 0.5 cm^{-1}.

Leonardite was solubilized at pH between 9 and 10 (adding 1 mol L^{-1} NaOH) to ensure complete dissolution.[42] Then, any possibly present HA molecules <10 kDa were removed using the Labscale TFF system equipped with a Pellicon XL membrane[43] (PLCGC10, Millipore). The dissolved organic carbon (DOC) concentrations were measured by the Carbon Analyzer (TOC-L CPH, Shimadzu). Further in this work, humic acid (HA) denotes leonardite for simplification purposes.

2.1.2. Cd adsorption edges

Adsorption edges were obtained using batch experiments in opaque plastic bottles to avoid any photoluminescence process. All plastic containers were acid-washed, and all reagents used were of reagent grade. Adsorption experiments with Cd ICP standard (Merck standard) were performed under N_2 atmosphere at three different initial metal concentrations (10^{-6}, 10^{-5}, and 10^{-4} mol L^{-1}) and three ionic strengths (10^{-1}, 10^{-2}, and 10^{-3} mol L^{-1} with $NaNO_3$ as a background electrolyte). The DOC concentration

was fixed for each batch experiment at 60 mg L^{-1}. A volume of 60 to 75 mL was used for each batch experiment, and the pH was buffered by adding a controlled volume of HNO_3 (10^{-1}, 10^{-2}, and 10^{-3} mol L^{-1}) and NaOH (10^{-1}, 10^{-2}, and 10^{-3} mol L^{-1}) ranging from 2 to 11 pH units. Each bottle was then closed and agitated for 24h. After equilibration, the pH was measured, and an aliquot of the sample (12 mL) was centrifuged using a centrifugal filter device at 6600 rpm for 45 minutes (Amicon® Ultra-15 centrifugal filter devices 3kDa). Before the ultrafiltration, the centrifugal filter device was washed with NaOH 0.05 mol L^{-1} and MilliQ® water to remove trace amounts of glycerin that could have interfered with the measurements. The filtrate was analyzed for Cd concentration using inductively coupled plasma optical emission spectroscopy (ICP OES; 720 Series, Agilent Technologies) or inductively coupled plasma mass spectroscopy (ICP-MS; iCAP Q, Thermo Fisher Scientific), depending on Cd concentrations. Cadmium bound to HA was calculated as the difference between the initial Cd concentration and the final Cd concentration in the filtrates.

2.1.3. Complexation modeling

The datasets of the adsorption edges were used further for the modeling using Visual MINTEQ software.[44] The NICA-Donnan model was used for our purpose, which results in a combination of non-ideal competitive adsorption (NICA) to a heterogeneous material, coupled with a Donnan electrostatic sub-model, describing the electrostatic attractions between ions and the humic material.[45–47] The distribution between the low adsorption sites (LAS, i.e., carboxylic sites) and high adsorption sites (HAS, i.e., phenolic sites) was calculated using the HH-10, i.e., leonardite HA, binding parameters[48] and the generic NICA-Donnan model parameters for Cd-ion binding by humic acids.[49] In our study, the thermodynamic NICA-Donnan model parameters for Cd-ion binding to HA were slightly modified (Table S1).

2.2. Cd isotope analysis

2.2.1 Batch experiments

Adsorption experiments with a Cd isotope standard (NIST SRM 3108 Cd) were performed under N_2 atmosphere at three fixed pH values (4, 5, and 6), three different initial metal concentrations (2×10^{-6}, 2×10^{-5}, and 2×10^{-4} mol L^{-1}), five ionic strengths (10^{-1}, 5×10^{-2}, 10^{-2}, 5×10^{-3}, and 10^{-3} mol L^{-1} with $NaNO_3$ as the background electrolyte). The DOC concentration (120 mg L^{-1}) was increased two times from previous batch experiments in order to obtain a sufficient amount of material for performing FTIR and XAS measurements. The initial concentration of Cd was also doubled to maintain the same Cd/HA ratio. In the case of 10^{-6} mol L^{-1} Cd, only two fixed pH values were used (4 and 5) as pH 6 did not allow us to analyze the small amount of Cd in the solution. The batch experiment conditions were similar to those used for the determination of the adsorption edges and HA was separated from the solution through a series of ultrafiltrations (five times 12 mL on the same centrifugal filter device 3 kDa) at 6600 rpm for 45 minutes. Cadmium concentrations and isotope compositions were measured in the solution samples. The HA fraction was recovered, freeze-dried, and used for EXAFS and FTIR measurements and for Cd isotope analysis (nine HA samples) to determine the isotopic mass balance. Kinetic batch complexation experiments were conducted to monitor the equilibration time of Cd isotope fractionation with HA at high (10^{-1} mol L^{-1} $NaNO_3$) and low (10^{-3} mol L^{-1} $NaNO_3$) ionic strengths with a Cd concentration of 10^{-5} mol L^{-1} and DOC concentration of 120 mg L^{-1}.

2.2.2. Cadmium isotopes measurements

Cadmium isotope ratios were measured using thermal ionization mass spectrometry (TIMS; Triton, ThermoFisher), and Cd isotopic compositions are reported as $\delta^{114/110}$Cd, relative to the NIST SRM 3108, with Eq. 1:

$$\delta^{114/110}\mathrm{Cd} = \left(\frac{\left(\frac{^{114}\mathrm{Cd}}{^{110}\mathrm{Cd}}\right)_{\mathrm{sample}}}{\left(\frac{^{114}\mathrm{Cd}}{^{110}\mathrm{Cd}}\right)_{\mathrm{NIST\ SRM\ 3108}}} - 1 \right) \times 1{,}000 \qquad (1)$$

Raw measurements were corrected for potential Cd isotope fractionation during the Cd purification procedure and the analysis, the double-spike (DS) method based on the nested iteration method was used. The DS was prepared by mixing two enriched Cd isotopes spikes: ^{106}Cd (97%) and ^{116}Cd (99 %) purchased from IsoFlex, USA. The DS was added to the sample before the Cd separation process and was composed of ^{106}Cd (35%) and ^{116}Cd (65%). The natural/DS ratio was 5.6 for $^{106}Cd/^{110}Cd$ and 10.8 for $^{116}Cd/^{110}Cd$.

Before the Cd separation process, liquid samples were evaporated and transferred to bromide form, whereas HA samples were firstly dissolved in a mixture of concentrated HNO_3 and H_2O_2 and then transferred to bromide form. Chromatographic separation of Cd was performed following the analytical methods previously published by Schmitt et al.[50,51] and Abouchami et al.[4,52] This technique was inspired by Pb separation and is promising because it is fast and requires only small amounts of acid. In comparison with Cd isotope measurements by MC-ICP MS, there were no isobaric interferences due to Sn and Pd isotopes,[51] allowing us to skip the chemical separation of Sn using a second anion-exchange chromatography. This protocol was adapted in our laboratory using 400 µL of the BioRad AG1-X8 anion exchange resin (100-200 mesh) in bromide form.

After Cd recovery, the sample was evaporated entirely on a hot plate (110-120°C) to the last drop. After cooling, an activator was added to the sample depending on the amount of Cd. For 500 ng of Cd, the activator was composed of 50 µL of H_3PO_4 0.1 N and 100 µL of silica gel (100 mg L^{-1} of Si). Then, the sample was evaporated to dryness and 10 µL of 2% HNO_3 was added and treated by ultrasonication. The volume was loaded stepwise onto outgassed single Re filaments. Peak emission of Cd ions occurs in the temperature range from 1150 to 1200 °C with this activator. The signal varied between 0.2 to 0.5 V (^{112}Cd, central cup) for the sample, and three complete measurements were feasible: 10 blocks of 20 cycles giving 600 measured values for the $^{114}Cd/^{110}Cd$ ratio.

Additionally, in order to evaluate the Cd purification procedure and the analysis, the full purification procedure was applied for standard solutions (BAM-I012 and NIST SRM 3108) and

international soil standard (NIST SRM 2711a Montana soil II). During the experiment and purification, the procedure blank was 4 pg of Cd, having a negligible impact on Cd isotopic composition. International reference standard solutions BAM I012 and NIST SRM 3108 were analyzed, and the long-term external precision was found to be ±0.08‰ (2SD, n=12) and ±0.02 ‰ (2SD, n=3), respectively. The measured $\delta^{114/110}$Cd value, relative to the NIST SRM 3108, was -1.32 ± 0.08‰ for BAM I012 (n=12, mean published value[53]: -1.33 ± 0.43‰) and 0.57 ± 0.02‰ for NIST 2711a Montana soil II (n=10, mean published value[54–56]: 0.55 ± 0.03‰).

2.3. Cd EXAFS measurements

The Cd XAS spectra were collected on the SAMBA beamline (SOLEIL Synchrotron, France) at the Cd K-edge (26.7 keV). The energy was calibrated by setting the first inflection point of a Cd metallic foil XANES. The reference (CdO) and samples were prepared as pellets of finely ground and homogenized powder with boron nitride (15 mg of sample + 45 mg of BN) and then sealed with Kapton tape and mounted in sample holders. The data were collected under vacuum at 20 K using a He cryostat to avoid modification in Cd speciation and sample damage due to beam exposure. Spectra were collected in transmission (using an ionization chamber) and fluorescence modes. According to the spectrum quality, several spectra (up to 30) were collected over the 26.65-27.70 keV energy range. Each raw bulk-XAS spectrum of Cd K-edge was merged and normalized, and the background was subtracted with a spline fitting function to obtain the extended X-ray absorption fine structure (EXAFS) function using Athena software.[57] Fourier transforms were generated on k^3-weighted spectra over *k*-ranges of 1.5-15 Å and 2-10 Å using the Hanning window for the reference (CdO) and samples, respectively. Theoretical backscattering-amplitude (S_0^2) and phase-shift (ΔE_0) values were calculated using FEFF 6.0 (IFEFFIT package) based on the crystal structure of CdO. The S_0^2 factor was set to 1.14159. The known structure of Cd acetate dihydrate[58] was used to find the structural parameters that best fit the observed spectrum for the HA samples. The goodness of fit was characterized by two parameters: the XAFS reliability factor R,

which measures how close the fit is to the experimental data, and the reduced χ^2 factor, which considers the number of floating parameters and noise in the data.

3. Results and discussion

3.1. Cadmium complexation with HA

Cadmium complexation with HA depends on the pH and ionic strength and is complete in the pH range of 3 to 7 (Fig. 1 and S2). At low ionic strength, low competition between Na^+ and Cd^{2+} leads to a complete Cd complexation in acidic and neutral conditions. On the other hand, at high ionic strength, strong competition between Na^+ and Cd^{2+} led to a complete Cd complexation only in neutral and alkaline conditions. Additionally, the influence of the Cd/DOC ratio highlights the diversity of HA binding groups, which are present in various proportions and cover a large range of affinity constants for Cd. The presence of few high-affinity sites and many weaker sites resulted in complete Cd complexation at lower pH levels for low Cd/DOC than for high Cd/DOC ratios (Fig. 1). Complexation of Cd-HA was investigated using 150 batch experiments under different experimental conditions (Cd concentration, ionic strength, and pH). This large experimental data set allowed us to precisely investigate and model Cd complexation with HA using the NICA-Donnan model.[45,47,59,60]

3.2. Cadmium speciation during complexation with HA

The NICA-Donnan model described four main Cd species (Fig. 2, S3, and S4): Cd^{2+} in solution (Cd^{2+}_{aq}), non-specifically bound Cd^{2+} (i.e., accumulated in the Donnan volume via electrostatic attractions, Cd^{2+}_{D}), Cd complexed with carboxylic groups (COO-Cd), and Cd complexed with phenolic groups (PhO-Cd). Furthermore, inorganic complexes, other than Cd^{2+} in solution, were only minor components of Cd aqueous speciation with contributions lower than 0.01% ($Cd(OH)^+$, $CdNO_3^+$, etc.).

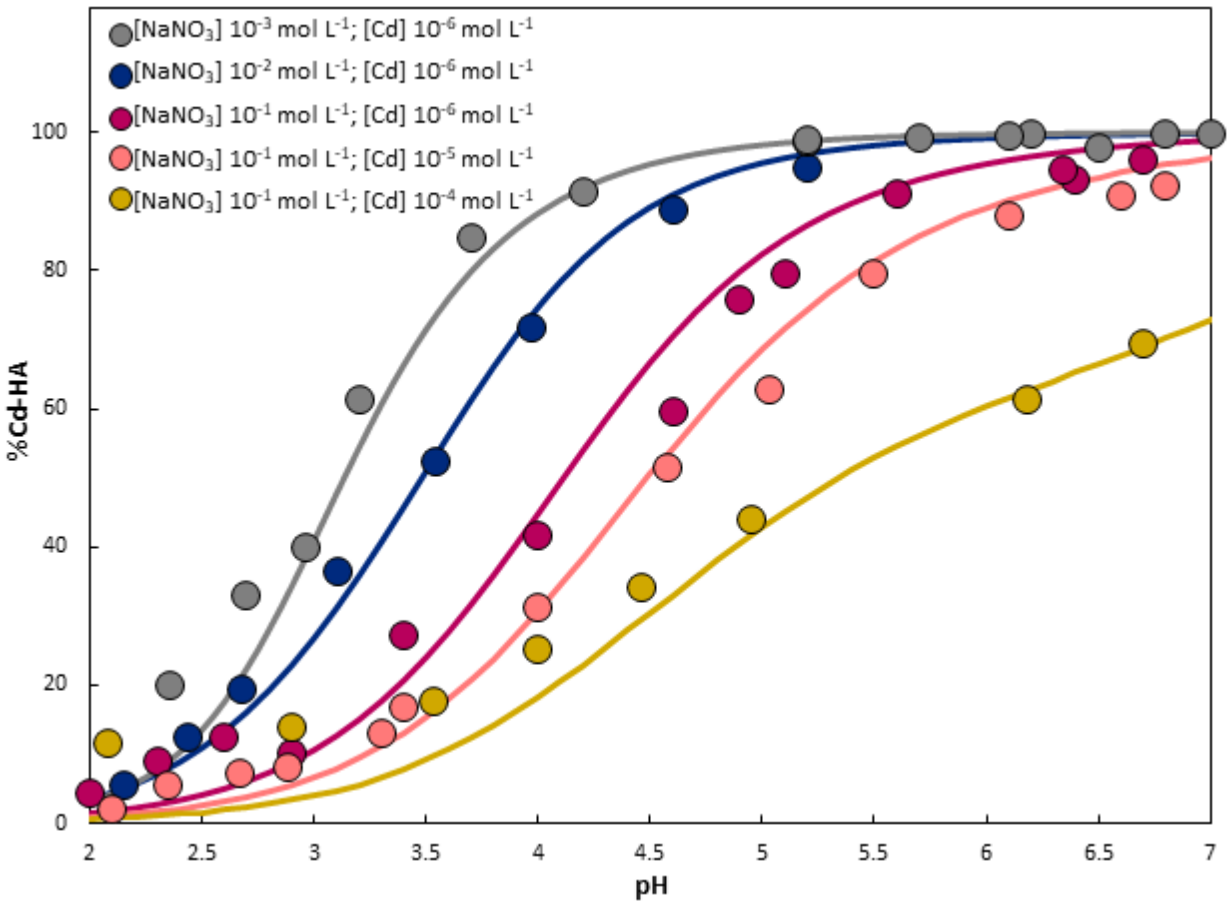

214

215 **Figure 1**: Cadmium complexation with HA (60 mg L^{-1} DOC) at different Cd concentrations and ionic
216 strengths ($NaNO_3$ as background electrolyte) and as a function of pH. Scatter plots express experimental
217 data, solid lines represent modeling by Visual MINTEQ (NICA-Donnan model). The ionic strength effect
218 on Cd complexation is highlighted at 10^{-6} mol L^{-1} Cd. The effect of the Cd concentration on the Cd
219 complexation is expressed at 10^{-1} mol L^{-1} $NaNO_3$. The remaining complexation dataset is shown in Figure
220 S2.

221 First, the formation of Cd(II)-carboxyl complexes[61] occurred in acidic and neutral conditions
222 because of the larger deprotonation of carboxylic groups compared with phenolic groups at low pH values
223 (Fig. 2a, S3a, and S4a). At low Cd concentrations (10^{-6} and 10^{-5} mol L^{-1}), carboxylic groups complexed at
224 least 80% of total Cd, while at a higher Cd concentration (10^{-4} mol L^{-1}), Cd complexation was limited to
225 60% due to (i) site saturation, (ii) charge neutralization of HA which led to less favorable electrostatic
226 attractions, and (iii) conformational changes of HA that limited the site availability for Cd
227 complexation[62,63] (Fig. 2a, S3a, S4a). Although phenolic groups are high-affinity sites for cations,[49] PhO-

Cd complexation was limited by the protonation of phenolic groups at pH levels between 2 and 7. Therefore, most of Cd complexation in the environment will occur at this pH range from 3 to 7 and will be mainly controlled by the carboxylic sites.

Secondly, ionic strength had a small effect on Cd complexation to carboxylic groups (Fig. 2b, S3b, S4b), but it strongly affected non-specific binding of Cd with HA. Indeed, due to its amphiphilic character, HA forms micelle-like structures[64] acting as electrically neutral phases with a consistent negative electrostatic potential (Donnan potential) compared to the solution.[65] On the other hand, the electrostatic potential is "neutralized" by the counterions from the background electrolyte Na^{+}_{aq} and Cd^{2+}_{aq} in solution.[45,66] As a result, the highest effect of electrostatic attractions between Cd and HA was observed at pH around 4 and at low ionic strength. In these conditions, the carboxylic sites are weakly deprotonated and the competition between Cd^{2+} and Na^{+} in the Donnan volume is low (Fig. 2). That led to a prevalence of non-specific Cd binding (up to 50% of total Cd, 60% of the total complexed Cd) due to electrostatic attractions. Furthermore, non-specific binding is almost absent in alkaline conditions, where phenolic and carboxylic groups are deprotonated and ionic strength too high. However, at high Cd concentrations, there are not enough deprotonated sites to bind all the Cd in solution and non-specific binding is still important at pH 6-7 corresponding to 35% of total Cd due to the saturation of the binding sites (Fig. S3).

Finally, thermodynamic modeling allowed us to specify Cd speciation. Over the pH range from 3 to 7, Cd speciation is explained by the relative proportions of complexation with carboxylic groups (COO-Cd), non-specific Cd binding in the Donnan volume (Cd^{2+}_{D}), and the free Cd species in solution (Cd^{2+}_{aq}). Consequently, the isotopic approach was designed to determine the Cd isotopic signature ($\delta^{114/110}Cd$) in the same experimental conditions (Table 1) and to characterize the Cd isotope fractionation associated with Cd binding to carboxylic groups or by electrostatic attractions.

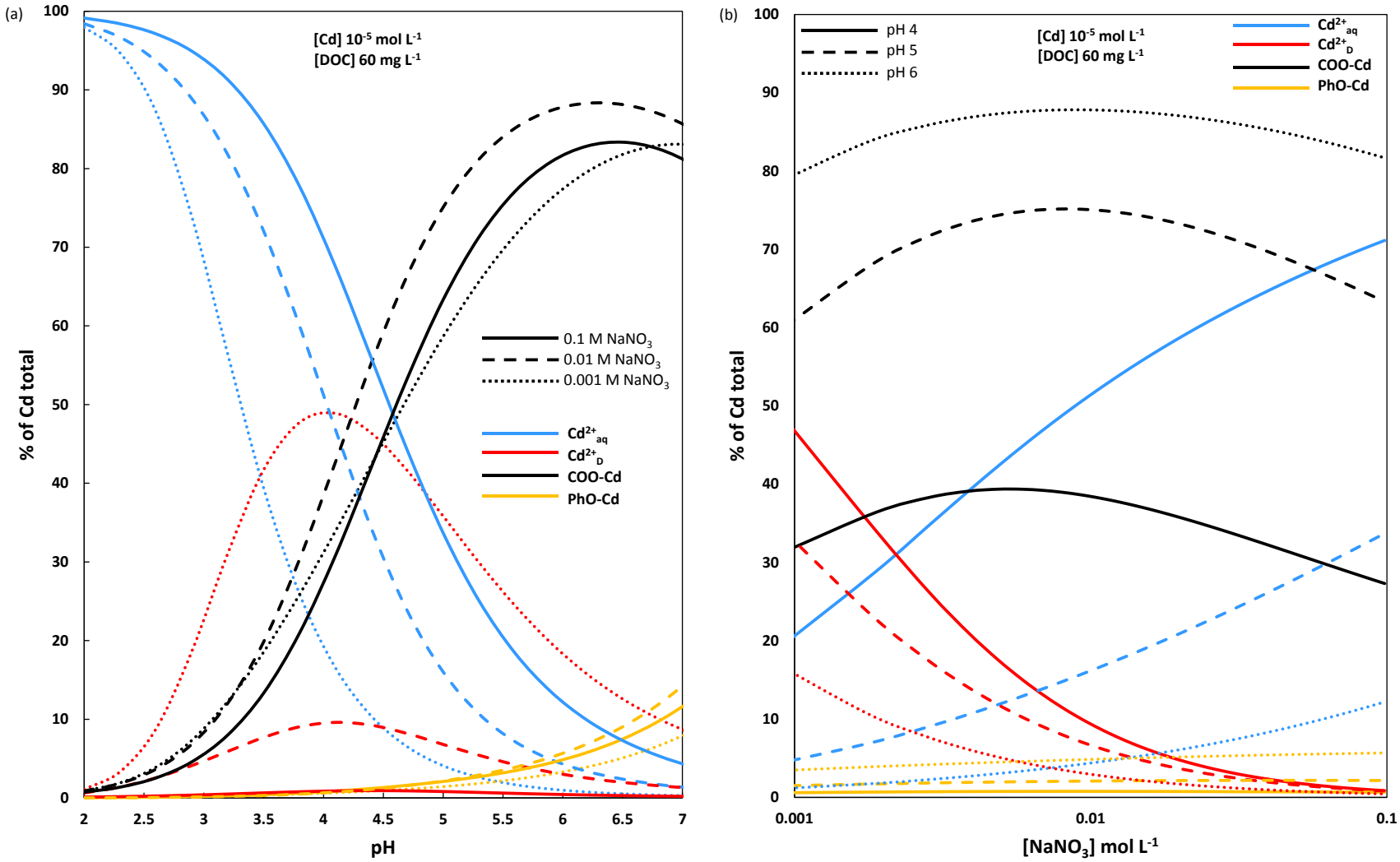

250

251 **Figure 2**: Cadmium speciation as a function of (a) pH and (b) ionic strength ($NaNO_3$). The data were determined using the NICA-Donnan model
252 for 10^{-5} mol L^{-1} Cd and 60 mg L^{-1} DOC. Cd^{2+}_{aq} refers to the aqueous Cd free in solution, Cd^{2+}_{D} to the Cd bound to HA by electrostatic attractions,
253 COO-Cd to the Cd complexed with carboxylic sites, and PhO-Cd to the Cd complexed with phenolic sites.

Table 1: Detailed experimental conditions and Cd isotope measurements in solution and in the HA fraction. The isotopic mass balance was calculated for 9 samples and did not exceed 0.03‰. The amount of Cd bound to HA by electrostatic attractions ($f(Cd^{2+}D)$) and with the carboxylic groups (f(COO-Cd)) and aqueous Cd in solution $f(Cd^{2+}aq)$ were calculated based on the NICA-Donnan chemical speciation modeling (n.d.: not determined).

	pH solution	[$NaNO_3$] mol L^{-1} solution	f(Cd) in solution	$f(Cd^{2+}_{aq})$ model.	$f(Cd^{2+}_{D})$ model	f(COO-Cd) model	$\delta^{114/110}$Cd solution (‰)		2 SD	$\delta^{114/110}$Cd solid (‰)		2 SD	Isotopic balance
[Cd] 2×10^{-4} mol L^{-1}; [DOC] 120 mg L^{-1}	4.2	1.0E-01	0.74	0.73	0.02	0.25	0.02	±	0.02	-0.06	±	0.01	0.00
	4.0	4.8E-02	0.72	0.74	0.03	0.23	0.02	±	0.02				
	4.0	9.8E-03	0.56	0.61	0.12	0.26	0.05	±	0.04				
	3.9	5.1E-03	0.53	0.57	0.19	0.24	0.06	±	0.04				
	4.0	1.1E-03	0.46	0.39	0.39	0.22	0.08	±	0.03	-0.04	±	0.04	0.02
	5.0	1.0E-01	0.55	0.53	0.02	0.44	0.03	±	0.04				
	5.0	4.7E-02	0.40	0.48	0.03	0.48	0.05	±	0.01				
	4.9	1.0E-02	0.30	0.37	0.12	0.50	0.08	±	0.00				
	4.9	5.3E-03	0.25	0.31	0.19	0.49	0.10	±	0.02				
	4.9	1.1E-03	0.20	0.17	0.42	0.41	0.12	±	0.02				
	6.2	1.0E-01	0.33	0.36	0.01	0.57	0.08	±	0.01	-0.01	±	0.03	0.02
	5.9	4.8E-02	0.25	0.34	0.03	0.59	0.09	±	0.01				
	6.0	9.5E-03	0.12	0.21	0.11	0.64	0.09	±	0.05				
	5.4	4.5E-03	0.14	0.21	0.20	0.57	0.13	±	0.01				
	5.8	1.1E-03	0.07	0.07	0.38	0.53	0.16	±	0.02				
[Cd] 2×10^{-5} mol L^{-1}; [DOC] 120 mg L^{-1}	4.0	1.0E-01	0.75	0.59	0.01	0.39	0.05	±	0.04	-0.10	±	0.03	0.01
	4.0	4.6E-02	0.61	0.51	0.03	0.45	0.04	±	0.01				
	4.0	1.1E-02	0.37	0.37	0.13	0.49	0.09	±	0.04	-0.01	±	0.08	0.03
	4.1	5.7E-03	0.26	0.27	0.21	0.52	0.12	±	0.04				
	4.0	1.2E-03	0.16	0.12	0.52	0.35	0.17	±	0.03				
	5.1	1.0E-01	0.37	0.20	0.01	0.76	0.07	±	0.02				
	5.1	5.1E-02	0.21	0.15	0.02	0.80	0.11	±	0.03				
	5.1	1.1E-02	0.09	0.09	0.07	0.82	0.13	±	0.04				
	5.0	4.9E-03	0.05	0.06	0.14	0.78	0.15	±	0.02				
	5.0	1.1E-03	0.02	0.02	0.36	0.61	0.19	±	0.04	0.01	±	0.09	0.01
	6.0	9.9E-02	0.15	0.07	0.00	0.87	0.11	±	0.02				
	6.0	5.2E-02	0.09	0.05	0.01	0.88	n.d.						
	6.0	1.0E-02	0.02	0.02	0.03	0.90	0.13	±	0.02				
	6.1	4.9E-03	0.02	0.01	0.05	0.89	0.14	±	0.01				
	6.0	1.2E-03	0.01	0.00	0.18	0.78	0.18	±	0.05	0.01	±	0.05	0.01
[Cd] 2×10^{-6} mol L^{-1}; [DOC] 120 mg L^{-1}	4.1	1.0E-01	0.54	0.36	0.01	0.61	0.08	±	0.02	-0.07	±	0.01	0.01
	4.1	4.6E-02	0.34	0.30	0.02	0.66	0.10	±	0.03				
	4.1	9.8E-03	0.18	0.18	0.08	0.71	0.14	±	0.02				
	4.2	4.7E-03	0.10	0.11	0.14	0.72	n.d.						
	4.2	9.8E-04	0.06	0.04	0.41	0.54	0.22	±	0.01				
	5.2	1.0E-01	0.20	0.08	0.00	0.86	0.10	±	0.02	0.00	±	0.04	0.02
	5.2	5.1E-02	0.12	0.06	0.01	0.88	0.12	±	0.05				
	5.2	9.9E-03	0.04	0.03	0.03	0.90	0.14	±	0.03				
	5.1	5.3E-03	0.02	0.02	0.05	0.88	0.19	±	0.04				
	5.2	9.5E-04	0.01	0.01	0.22	0.75	n.d.						

3.3. Cd isotope fractionation during complexation with HA

The amount of Cd complexed with HA ranged from 25 to 99% of total Cd in solution (Table 1). After experiments, the $\delta^{114/110}$Cd values in solution varied from 0.02 ± 0.02‰ to 0.22 ± 0.01‰, showing preferentially enrichment in light Cd isotopes in the complexed form. The kinetic experiments demonstrated that the Cd isotopic composition was constant throughout the experiment at high ionic strength and that a plateau was rapidly reached after 5 hours at low ionic strength (Fig. S5). Therefore, we can assume that Cd complexation with HA reached isotopic equilibrium in the experimental conditions (Fig. 3). The overall Cd isotope fractionation was defined as $\Delta^{114/110}Cd_{HA\text{-}Cd(aq)}$ of -0.15 ± 0.01‰. Oppositely, previous research on the complexation of other metals belonging to the first raw transition (Cu, Fe, and Zn) showed an enrichment in heavy isotopes bound to HA. These observations were attributed to their stronger binding in organocomplexes than in aqueous solution at equilibrium.[67–70] Cadmium does not undergo natural redox reactions in such settings, leading us to hypothesize that the isotope fractionation was driven by differences in Cd coordination chemistry between the dissolved species and the complexed species. In our case, Cd complexation is driven by carboxylic sites and the electrostatic attractions, which may cause different Cd isotope fractionations as demonstrated for Cu with HA,[69], and in other systems for Zn.[71,72]

Consequently, this study highlights the importance of modeling to set up the experimental conditions, which included: (i) pH variations from 4 to 6, (ii) ionic strengths variations from 10^{-3} mol L^{-1} to 10^{-1} mol L^{-1}, and (iii) Cd concentrations in solution varying from 10^{-6} mol L^{-1} to 10^{-4} mol L^{-1}. By including all of these conditions, we had enough controlled data to determine Cd isotope fractionation associated with its complexation with carboxylic groups ($\Delta^{114/110}Cd_{(COO\text{-}Cd)\text{-}Cd(aq)}$) and that of the electrostatic attractions ($\Delta^{114/110}Cd_{(Cd2+D)\text{-}Cd(aq)}$).

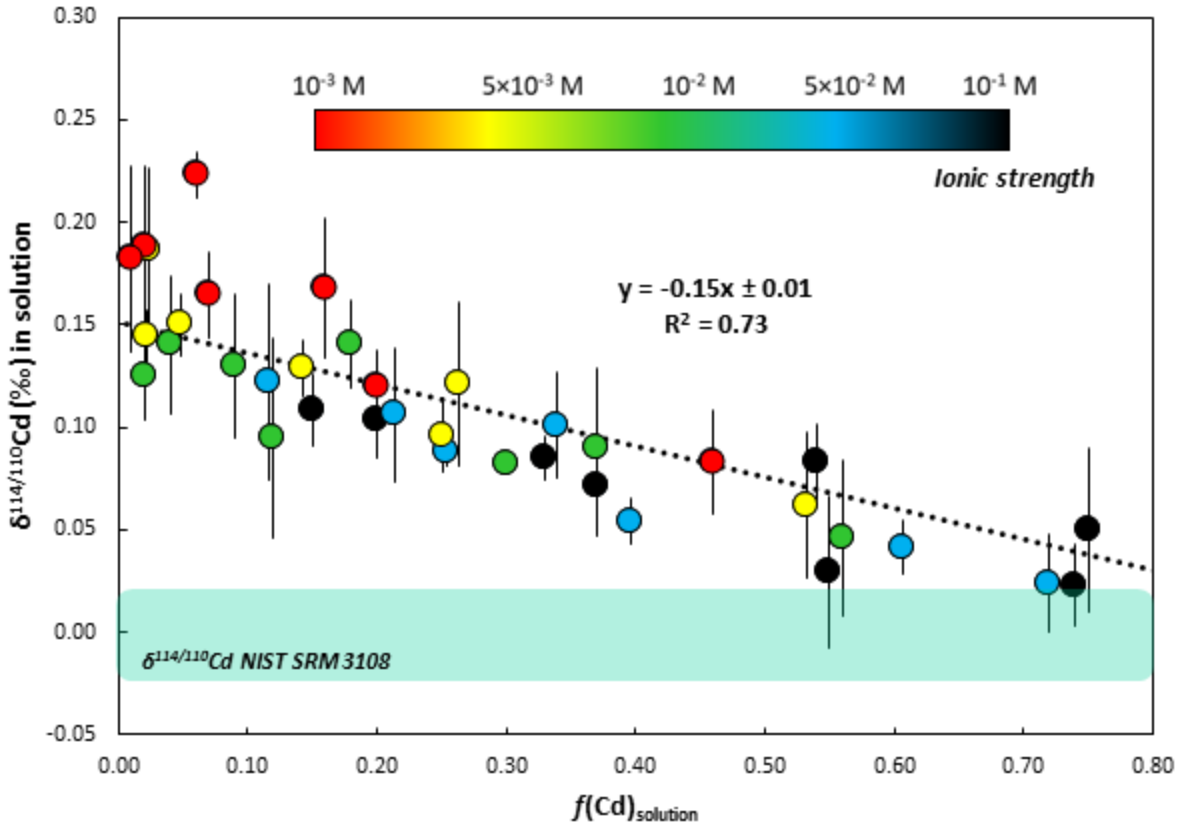

281

282 **Figure 3**: $\delta^{114/110}$Cd values (‰) in solution as a function of the remaining Cd in solution (f(Cd)) at
283 different ionic strengths and Cd concentrations (10^{-6} mol L^{-1}, 10^{-5} mol L^{-1} and 10^{-4} mol L^{-1}) after 24 h of
284 equilibration. Error bars on the y axis refer to 2SD. *The* graphical estimation gives an overall $\Delta^{114/110}Cd_{HA\text{-}Cd(aq)}$ = -0.15 ± 0.01‰ for the samples, with a linear regression set to 0.00‰ for f(Cd) value of 1 (black
286 dashed line). The slope uncertainty (±0.01) was determined by the least-squares method. The green
287 shading shows the isotopic range of the bulk starting composition (NIST SRM 3108).

288 **3.3.1. Specific Cd complexation: carboxylic sites**

289 The proportion of Cd complexed with carboxylic sites was determined based on the NICA-
290 Donnan thermodynamic modeling (Table 1). At high ionic strengths, Cd complexation was primarily
291 dependent on the carboxylic groups (Cd^{2+}_D lower than 3% of the total Cd and a ratio Cd^{2+}_D/COO-Cd lower
292 than 0.07 (16 samples). In these conditions, fifteen $\delta^{114/110}$Cd values in solution were related to Cd
293 complexation with the carboxylic sites, which represents a preferential enrichment in light isotopes bound
294 to HA following a linear regression (slope: -0.13 ± 0.01, R^2=0.80, Fig. S6). Therefore, the $\Delta^{114/110}Cd_{(COO\text{-}}$

295 $_{Cd)\text{-}Cd(aq)}$ was estimated to -0.13 ± 0.01‰. As an alternative to the graphical evaluation,[69] $\Delta^{114/110}Cd_{(COO\text{-}Cd)\text{-}}$

296 $_{Cd(aq)}$ can be calculated with Eq. 2 and 3

297 $$\Delta^{114/100}Cd_{\text{final solution-starting solution}} = \delta^{114/110}Cd_{\text{final solution}} - \delta^{114/110}Cd_{\text{starting solution}} \quad (2)$$

298 $$\Delta^{114/110}Cd_{(COO\text{-}Cd)\text{-}Cd(aq)} = -\Delta^{114/110}Cd_{\text{final solution-starting solution}} \Big/ \%(COO\text{-}Cd) \times 100 \quad (3)$$

299 where $\delta^{114}Cd_{\text{starting solution}}$ is the measured isotope composition of the starting solution. The $\delta^{114}Cd_{\text{final solution}}$ is

300 the measured isotope composition of the solution at the end of the complexation experiment, and %(COO-

301 Cd) is the percentage of the Cd complexed with carboxylic groups. The calculation resulted in a mean

302 $\Delta^{114/110}Cd_{(COO\text{-}Cd)\text{-}Cd(aq)}$value of -0.12 ± 0.03‰ (2SD, n=16).

303 As a consequence, the preferential enrichment in light Cd isotopes bound to HA demonstrated that

304 the dominant species of dissolved Cd likely have more stable bonds than those in the complexed form.[73,74]

305 The calculated Cd-O distances for the most common aqueous form ($Cd(H_2O)_6^{2+}$), either using the density

306 functional theory,[75] X-ray diffraction,[76] or RHF/DZP,[77] range from 2.29 to 2.34 Å. Moreover, the Cd-O

307 distances in perchlorate or nitrate solution vary from 2.28 to 2.31 Å with an octahedral geometry and

308 depend on the thermal effect during XAS measurements.[76,78–81] In our study, the Cd K-edge EXAFS

309 spectra for Cd bound to HA were successfully fitted with first shell coordination of the Cd complexed to

310 HA with an average Cd-O length of 2.29 Å (Fig. S7). Therefore, based on the numerous studies dealing

311 with Cd in solution, we agree that a slight change of the Cd-O first coordination does not permit to

312 confirm that carboxylic groups might express longer and thus weaker bonds than in an aqueous solution.

313 According to Koopal et al.[47], the thermodynamic parameter "nCd/nH" is interpreted as the

314 stoichiometry of the binding reaction (Table S1). The ratio of 0.9 indicates that the average stoichiometry

315 of Cd binding with carboxylic groups[82,83] (with respect to the proton reaction) is mainly monodentate.

316 Therefore, the obtained value (2.29 Å), which represents the average value of six Cd-O in the first Cd

317 coordination shell, does not differ from the established Cd-O lengths obtained from Cd solution

318 species.[76,78–81] In contrast, S ligands leading to significant coordination changes[84,85] induce an apparent Cd

isotope fractionation.[81,86] As a consequence, the coordination of carboxylic groups to Cd in monodentate fashion led to similar bond distances to water oxygens than in solution. Therefore, a significant isotopic shift would be observed as a result of a bidentate or multidentate Cd complex. Based on the fact that bond strength is related to bond length[87,88], the preferential presence of heavier Cd isotopes in the solution cannot be explained only by their smaller Cd-O length than those bound to HA.

Monodentate binding to negatively-charged oxygen donor atoms (phenolic and carboxylic functional groups) and the associated linear free energy relationships (LFER) for metal-ligand complexation led to a different behavior for Cd than for metals of the first transition raw.[89] Contrary to the metals from the first raw transition, Cd^{2+} may be subjected to a larger extent to outer-sphere complex prior formation with a ligand in an aqueous solution.[90,91] Indeed, Cd-ligand (L^-) overall complexation can be described by the following two equilibrium reactions:

$$[Cd(H_2O)_n]^{Z+}+L^- \rightleftharpoons [Cd(H_2O)_n\cdots L]^{(Z-1)+} \quad (4)$$

$$[Cd(H_2O)_n\cdots L]^{(Z-1)+} \rightleftharpoons \left[Cd(H_2O)_{n-1}L\right]^{(Z-1)+} + H_2O \quad (5)$$

where $[Cd(H_2O)_n\cdot\cdot\cdot L]^{(Z-1)+}$ denotes an outer-sphere complex, in which the ligand forms hydrogen-bonds with water molecules in the first coordination sphere of Cd^{2+}, and $[Cd(H_2O)_{n-1}L]^{(Z-1)+}$ is the inner-sphere complex in which one water molecule is replaced by the ligand in the first coordination sphere of Cd^{2+}. Therefore, Cd bound to carboxylic groups includes $[Cd(H_2O)_{n-1}L]^{(Z-1)+}$ and $[Cd(H_2O)_n\cdot\cdot\cdot L]^{(Z-1)+}$.

Moreover, theoretical calculations showed that the reduced partition function ratio (RPFR) $10^3\ln(\beta_{114\text{-}110})$ of the Cd hydration complexes increased with the increase of the number of water molecules, suggesting that the change in the hydration complexes (4, 5, or 6) may be a significant factor for isotope fractionation in solution.[75] The isotopic offsets in $\delta^{114/110}Cd$ ($\Delta^{114/110}Cd_{\text{hydration complexes}}$) can be estimated using the subtraction of one RPFR from another[75] (Eq. 6).

$$\Delta^{114/110}Cd_{\text{hydration complexes}}=\delta^{114/110}Cd(H_2O)_{n-1}-\delta^{114/110}Cd(H_2O)_n=10^3\ln\beta_{114\text{-}110}\,Cd(H_2O)_{n-1}-10^3\ln\beta_{114\text{-}110}\,Cd(H_2O)_n \quad (6)$$

The isotopic Cd shift is more pronounced at low temperatures. At 25°C, the RPFR exhibited 2.299, 2.261, and 2.167 for $Cd(H_2O)_6^{2+}$, $Cd(H_2O)_5^{2+}$, $Cd(H_2O)_4^{2+}$, respectively.[75] These results demonstrated that the lighter Cd isotopes were less stable and thus more susceptible to release a water molecule (inner-sphere complex) leading to the preferential enrichment of lighter Cd isotopes in the HA fraction. Moreover, X-ray absorption spectroscopy (XAS) studies on Cd coordination in solution revealed that Cd^{2+} could primarily occur as a $Cd(H_2O)_7^{2+}$ aqueous complex.[92–94] Therefore, Cd hydration complex in the aqueous solution is crucial in deciphering the isotope fractionation during its complexation and for Cd isotope systematics in environmental studies in general.

3.3.2. Non-specific Cd binding: electrostatic attractions

In addition to the role of carboxylic groups in Cd complexation, the electrostatic attractions also played a major role in the total Cd complexation with HA, especially at low ionic strengths and low pH values (Fig. 2, S3, and S4). Cadmium isotope fractionation plotted as a function of the Cd/Na molar ratio in solution followed a logarithmic regression exhibiting slopes increasing from 0.02 to 0.09 with decreasing Cd/Na molar ratio, with the R^2 factor ranging from 0.66 to 0.99 (Fig. 4).

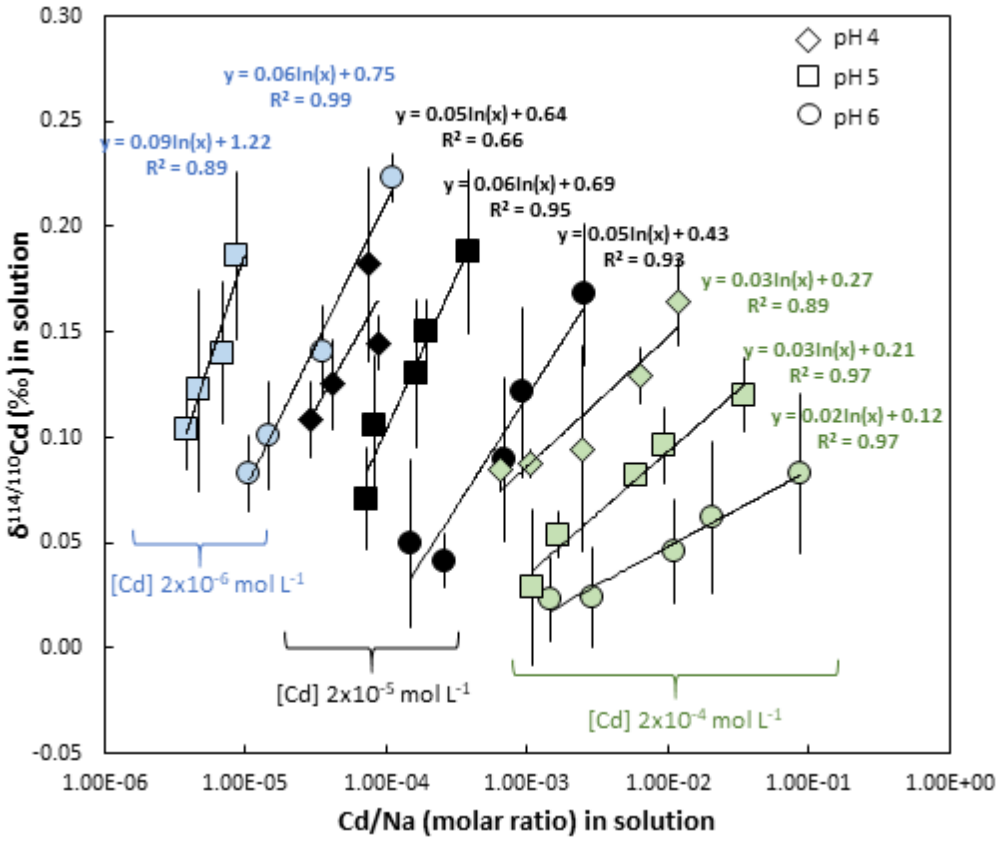

Figure 4: Cadmium isotopic composition ($\delta^{114/110}$Cd expressed in ‰) in solution as a function of Cd/Na (molar ratio) in solution at the beginning of the experiment. At each pH and each [Cd] in solution, the experimental data follows a logarithmic regression expressed by the equation and the R^2 factor. The error bars represent the analytical error (2SD).

Prior to this study, the exact influence of non-specific binding induced by electrostatic attractions on metal isotope fractionation has never been studied during metal complexation with HA. The complexation of Zn with HA, despite a low ionic strength (2×10^{-3} mol L^{-1}), has shown that electrostatic attractions represent only a small proportion of Zn bound to HA and therefore not capable to cause a measurable isotope fractionation.[68] The same observation has been noted for Cu at high ionic strength (10^{-1} mol L^{-1}), where electrostatically adsorbed Cu represented only a minor part (0.1-1%) of total Cu bound to HA.[69] However, our results showed that the proportion of Cd complexed by electrostatic attractions reached up to 50% of the total Cd, corresponding to 60% of the total complexed Cd (Fig. 2). Based on the Cd isotopic composition measured in solution and the Cd isotope fractionation attributed to the carboxylic

complexation, an isotopic mass balance calculation can be used to estimate the effective fractionation coefficient induced by electrostatic attractions with Eq. 7 and 8:

$$\Delta^{114/110}Cd_{x-y} = \delta^{114/110}Cd_x - \delta^{114/110}Cd_y = 1{,}000\ln\left(\alpha_{x-y}\right) \quad (7)$$

$$\alpha_{x-y} = \frac{\delta^{114/110}Cd_x + 1{,}000}{\delta^{114/110}Cd_y - 1{,}000} \quad (8)$$

where x represents Cd^{2+}_{aq} and y represents COO-Cd and Cd^{2+}_{D}; with their associated fractionation coefficient $\alpha_{(COO\text{-}Cd)}$ and $\alpha_{(Cd^{2+}_{D})}$, respectively. According to our previous results, we defined $\alpha_{(COO\text{-}Cd)}$ as 1.00013 and the $\alpha_{(Cd^{2+}_{D})}$ was determined by the least-squares method to model the $\delta^{114/110}Cd$ values in solution with Eq 9:

$$\delta^{114/110}Cd_{\text{modeled solution}} = -1{,}000f\left[\frac{P_{COO\text{-}Cd}\times\left(\alpha_{(COO\text{-}Cd)}-1\right)}{1-f+(f\times\alpha_{(COO\text{-}Cd)})} + \frac{P_{Cd^{2+}_{D}}\times\left(\alpha_{(Cd^{2+}_{D})}-1\right)}{1-f+(f\times\alpha_{(Cd^{2+}_{D})})}\right] \quad (9)$$

where *f* is the total fraction complexed with HA, $P_{COO\text{-}Cd}$ and $P_{Cd^{2+}_{D}}$ are the proportions of each site in total complexed Cd, and $\alpha_{(COO\text{-}Cd)}$ and $\alpha_{(Cd^{2+}_{D})}$ are their respective fractionation coefficients.

Therefore, the best agreement between the measured $\delta^{114/110}Cd$ values in solution and modeled $\delta^{114/110}Cd$ values determined an $\alpha_{(Cd^{2+}_{D})}$ of 1.00025, giving a $\Delta^{114/110}Cd_{Cd^{2+}_{D}\text{-}Cd(aq)}$ of -0.25‰ (Fig. 5). Surprisingly, the electrostatic attractions induced more extensive isotope fractionation than Cd complexation with carboxylic groups. However, when Cd complexation with carboxylic groups led to an inner-sphere complex, the electrostatic attractions were likely caused by a dipole-ion attraction between the Cd cation and the dipole of the oxygen from the OH responsible for an outer-sphere interaction.

Under such conditions, the electrostatic bonds are weak, and the Cd coordination number (complexation or hydration complexes) or Cd-HA bond lengths will not be modified relatively to the aqueous form of Cd. Therefore, there is no reason that such process induces Cd isotope fractionation. We also show the modeled $\delta^{114/110}Cd$ values in solution with a value of $\alpha_{(Cd^{2+}_{D})}$ set to 1, signifying that electrostatic attractions do not produce measurable Cd isotope fractionation (Fig. S8), which led to an underestimation of the measured $\delta^{114/110}Cd$ values at lower ionic strengths.

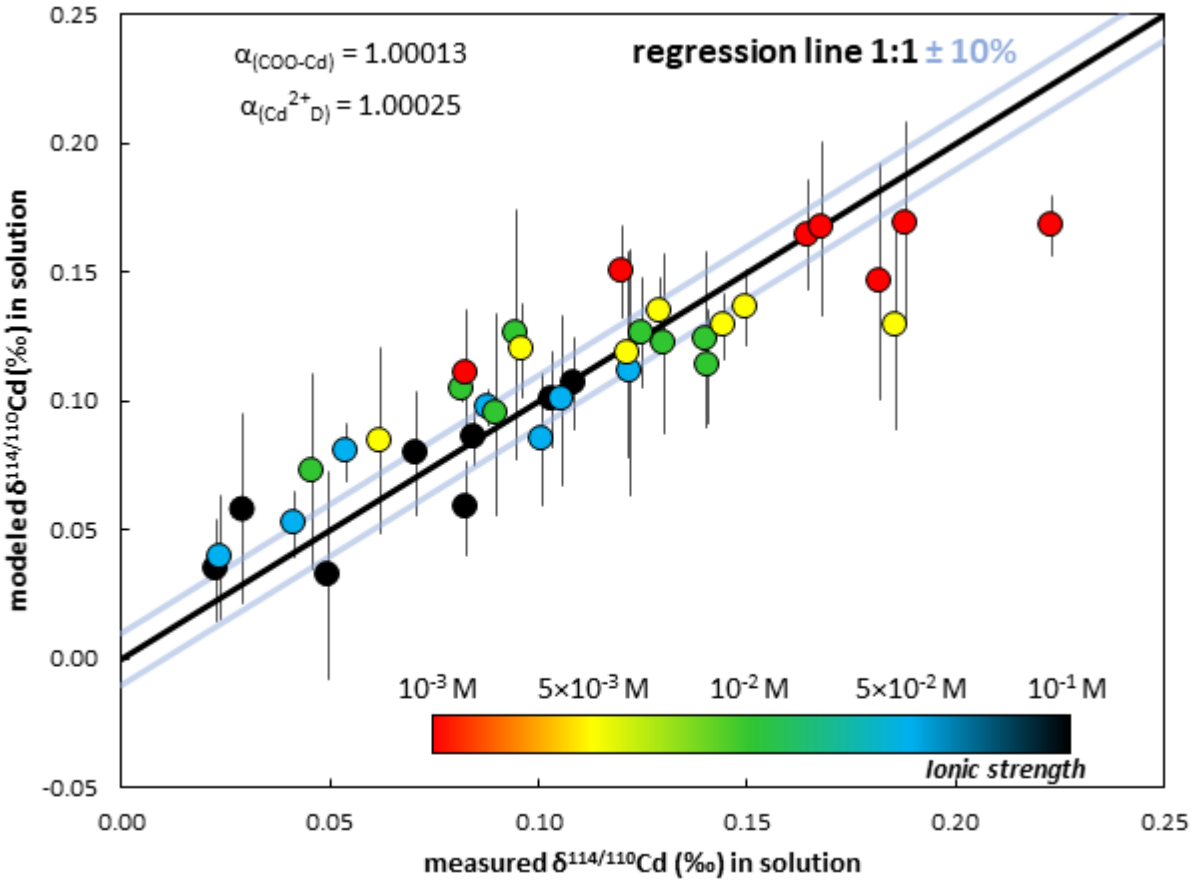

394

395 **Figure 5**: Comparison between measured $\delta^{114/110}$Cd in solution and modeled $\delta^{114/110}$Cd through isotopic
396 mass balance calculation (Eq. 8) for $\alpha_{(COO\text{-}Cd)}$ of 1.00013. and $\alpha_{(Cd^{2+}{}_{D})}$ of 1.00025. The $\alpha_{(Cd^{2+}{}_{D})}$ was
397 determined by the least-squares method. The black line represents the linear regression 1:1 with a range of
398 10% (grey lines). The error bars represent the analytical error (2SD).

399 Therefore, a $\Delta^{114/110}Cd_{Cd^{2+}{}_{D\text{-}Cd(aq)}}$ of -0.25‰ has to be applied to Cd isotopes fractionation during
400 the complexation with HA. Humic acids are large and negatively charged polyelectrolytes, which results
401 in the accumulation of cations in the vicinity of HA binding sites, leading to different chemical conditions
402 between the solution and the vicinity of HA. Electrostatic models[95] (Nica Donnan, Donnan-EV, Donnan-
403 EDL model, etc.) aim at converting the dissolved cation concentration in the bulk solution ($[C]_i$) to a local
404 dissolved cation concentration ($[C]_{loc,i}$) that occurs adjacent to the HA site, calculated according to the
405 Boltzmann's law with Eq. 10:

$$[C]_{Cd_D^{2+}} = [C]_{Cd_{aq}^{2+}} \times exp\left(-\frac{z(Cd2+)F\Psi}{RT}\right) \quad (10)$$

where z(Cd^{2+}) is the valence of Cd, F is the Faraday constant, Ψ is the electrostatic potential of HA particles, R is the gas constant, and T is the absolute temperature. This effect is calculated using the Boltzmann factor (Bf) with Eq. 11:

$$Bf = \frac{[C]_{Cd_D^{2+}}}{[C]_{Cd_{aq}^{2+}}} \quad (11)$$

The $\Delta^{114/110}Cd_{HA\text{-}Cd(aq)}$ calculated (Eq. 12), based on measured $\delta^{114/110}Cd$ value and the verified isotopic mass balance (Table 1), was expressed as a function of the Bf (Fig. 6).

$$\Delta^{114/110}Cd_{HA\text{-}Cd(aq)\ calculated} = (\delta^{114/110}Cd_{initial} - f(Cd_{aq}) \times \delta^{114/110}Cd_{solution})/(1 - f(Cd_{aq})) - (\delta^{114/110}Cd_{solution}) \quad (12)$$

where $f(Cd_{aq})$ is the proportion of Cd in the aqueous form in solution and $\delta^{114/110}Cd_{initial}$ is set to 0‰.

At low Bf, isotope fractionation is limited, and the $\Delta^{114/110}Cd_{HA\text{-}Cd(aq)}$ is controlled by carboxylic complexation. However, at high Bf, the strongest isotope fractionation is observed, related to the non-specific Cd binding during electrostatic attractions. As a result, these must play a significant role in Cd isotope fractionation during complexation with HA. As previously observed for Zn sorption onto kaolinite,[72] the mechanism leading to preferential lighter Cd isotope enrichment during outer-sphere complexation formation *via* electrostatic attractions remains unclear and additional studies are required to explain the effect of electrostatic attractions on metal isotope fractionation.

In general, Cd isotope fractionation is controlled by pH and ionic strength and occurs throughout specific complexation processes with the carboxylic sites and non-specific Cd binding induced by electrostatic attractions. Based on our large experimental dataset, the overall Cd isotope fractionation due to Cd complexation with HA can be set for future studies as a $\Delta^{114/110}Cd_{HA\text{-}Cd(aq)}$ of -0.15 ± 0.01‰.

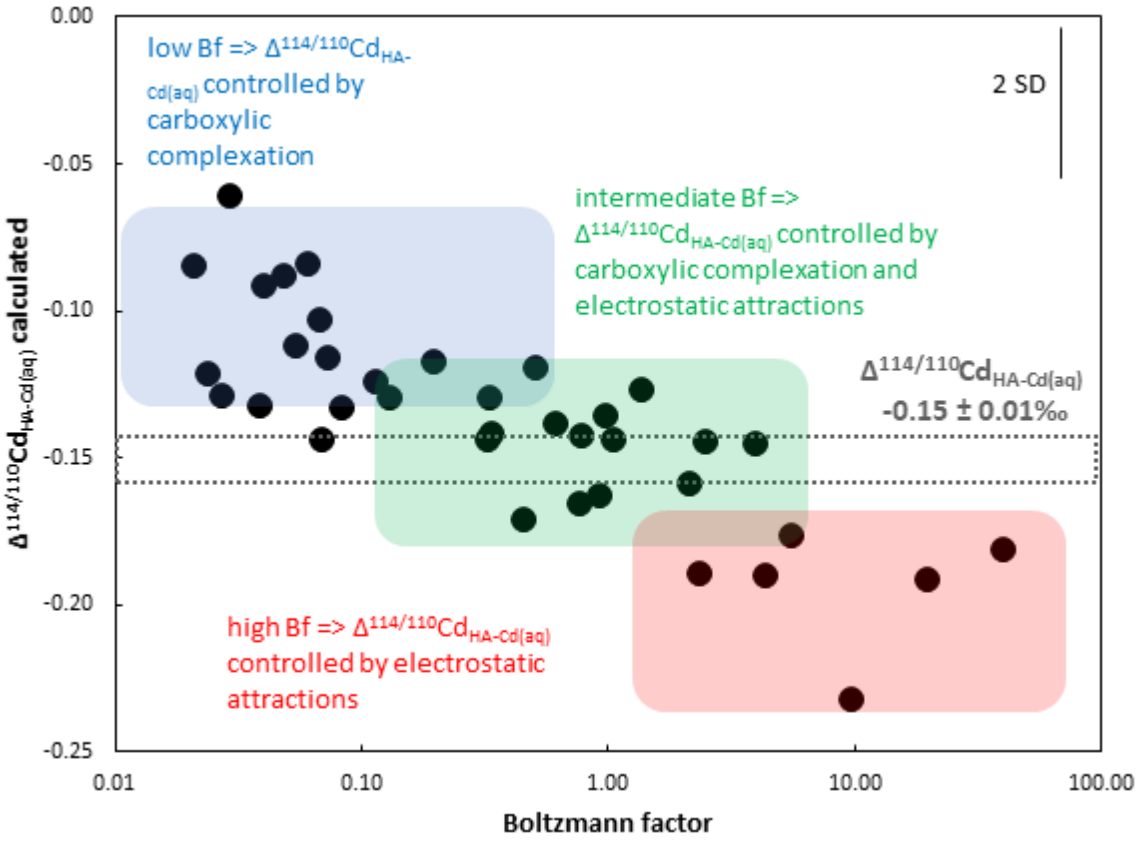

Figure 6: $\Delta^{114/110}Cd_{HA\text{-}Cd(aq)}$ calculated as a function of the Boltzmann factor (Bf). The error bar represents the highest analytical error observed for one measured $\delta^{114/110}Cd$ value (2SD). The grey rectangle represents the overall Cd isotope fractionation due to Cd complexation with HA as $\Delta^{114/110}Cd_{HA\text{-}Cd(aq)}$ = -0.15 ± 0.01‰.

4. Environmental implications

Our study is an important contribution to Cd isotope systematics focusing on Cd complexation with HA, an important constituent in soils, sediments and waters. Information on Cd isotope fractionation after complexation with natural organic matter is crucial to fully understand the biogeochemical processes in the Cd-soil-aqueous solution-plant continuum and for contamination tracing. The introduction of Cd to the soil environment and its initial solubilization is followed by numerous biogeochemical reactions with soil components. Modeling Cd speciation in soil solution revealed that dissolved Cd is present either bound to dissolved organic matter (DOM) or as free Cd^{2+}.[86] Based on our data on Cd isotope fractionation

after complexation with the carboxylic sites and bound to HA by electrostatic attractions, we show that free Cd^{2+}, which is the main form taken up by the plants,[96] should be preferentially enriched with the heavier isotopes compared to Cd bound to soil organic matter, as assumed in a previous study.[86] These findings are in accordance with the heavier Cd isotope pool available for crops and Cd hyper-accumulating plant species.[8–11,86] However, when environmental factors change, e.g., pH and Eh due to flooding, contaminants input, soil organic matter quantity and quality, ionic strength of the soil solution, etc., changes of Cd sorption/desorption occurs as a result of the competition of negatively charged sites, and the Cd isotope composition may thus be strongly modified. In order to completely understand Cd behavior in the soil environment, studies involving other soil constituents, and their affinity to Cd, are required. Moreover, a comparison of our study with HA analogs (plants, phytoplankton, diatoms, etc.) would allow explaining simple complexation mechanisms, although we are aware of the fact that limiting the conclusions to these simple processes might be a simplification.

Cadmium is mainly coordinated with O atoms[97,98] in plant tissues of Cd hyperaccumulators, as determined by Cd K-edge EXAFS spectroscopy. Additionally, Ueno et al.[99] and Tian et al.[100] found that in Cd hyperaccumulators leaves, Cd was present in an octahedral coordination with O ligands, possibly due to the presence of malate and citrate. Therefore, the complexation of Cd with malate and citrate in the leaves, i.e., carboxylic ligands, might be responsible for the preferential enrichment in light isotopes. Recent development of Cd isotope measurements in the ocean provides new clues for identifying the key mechanisms controlling the Cd biogeochemical cycle in surface ocean. While the effect of uptake by phytoplankton on $\delta^{114/110}Cd$ signatures has been shown in nutrient repleted regions,[4,101] the impact of organic complexation is still debated, namely for its buffering effect on the $\delta^{114/110}Cd$ measured in nutrient-depleted waters.[102] In surface seawater, Cd aqueous speciation is dominated by Cd-organic complexes.[103–105] Thus, the dissolved $\delta^{114/110}Cd$ is similar to those complexes. Previous research has shown that Cd organic complexation only occurs via surface complexation since the 0.5 mol L^{-1} mean ionic strength of seawater prevents any electrostatic attractions. Louis et al.[106] showed that dissolved organic matter sampled in the Mediterranean Sea off the coast of France is composed of 60% carboxylic and 40%

phenolic sites, in agreement with the overall binding site composition of the HA used in this study. Therefore, based on the relatively small value of $\Delta^{114/110}Cd_{(COO\text{-}Cd)\text{-}Cd(aq)}$ = -0.13‰ determined in our study, only a minor change of dissolved oceanic $\delta^{114/110}Cd$ can be associated with organic complexation. The isotopic shift is even smaller than the Cd isotope partitioning between Cd inorganic species ($\Delta^{114/110}Cd$ of 0.3‰ for $Cd^{2+}/CdCl_2$).[18]

In addition to organic ligands, phytoplankton-derived debris found as particles in the surface ocean can act as a Cd sink via surface complexation. After diatom remineralization, Cd adsorption occurring on the remineralization-resistant *Dunaliella tertiolecta* surface leads to a limited $\Delta^{114/110}Cd$ fractionation of -0.1 ± 0.1‰.[5] Furthermore, Pokrovsky et al.[107] and Gélabert et al.[108] have shown that carboxyl functional groups are responsible for more than 90% of total bound Zn and the behavior of Cd is similar to Zn since these two metals share the same geochemical traits. Therefore, our observations of limited Cd isotope fractionation during complexation with carboxylic groups is totally consistent with previous studies and strengthens the limited impact of Cd scavenging on the distribution of Cd isotopes during diatom mineralization.

As a conclusive remark, in nutrient-rich regions, the impact of organic complexation on $\delta^{114/110}Cd$ in surface oceanic waters is secondary with respect to Cd uptake by phytoplankton, which tends to enrich the dissolved $\delta^{114/110}Cd$ with preferentially heavier isotopes ($\Delta^{114/110}Cd_{surface\text{-}deepwater}$ up to 2.5‰).[4,52,101] However, in oligotrophic environments, stable and light $\delta^{114/110}Cd$ were measured at picomolar Cd concentrations.[102,109] As reported before, due to the predominance of the Cd-organic complexes in the dissolved fraction, dissolved $\delta^{114/110}Cd$ is directly driven by the Cd-organic fraction. The absence of heavier $\delta^{114/110}Cd$ linked with Cd biological uptake in such context indicates a buffering effect of the Cd-organic complexes in solution as proposed recently by Xie et al.[102] and Guinoiseau et al.[6] for the Atlantic Ocean transects. So, even if a small isotope fractionation is observed during Cd organic complexation, the importance of these organic complexes on the Cd oceanic cycle in metal-depleted water masses can be indirectly indicated using Cd isotopes.

Acknowledgements

The authors are thankful for the support from the Czech Science Foundation (18-07585S). The authors also acknowledge Marie Králová, Adéla Šípková, Andrea Žitková, Aleš Vaněk, and Petra Vokurková for their assistance in the laboratories and chemical measurements. James Tuffano is acknowledged for English editing. The synchrotron session at SOLEIL was partly funded by the European Framework Program for Research and Innovation (CALIPSOplus). The authors thank the SAMBA beamline staff for their support. The authors would also like to thank Stephen J.G. Galer (Max Planck Institute for Chemistry, Mainz-Germany) for his helpful advice regarding the Cd separation protocol and TIMS measurements. Rémi Marsac was supported by the C-FACTOR project funded by ANR (project number ANR-18-CE01-0008). Damien Guinoiseau is financially supported by the ANR RECA (project number ANR-17-CE01-0012). Three reviewers and the editor, Dr. Thomas B. Hofstetter, are acknowledged for their constructive comments and for significantly improving the quality of the manuscript.

Author Contributions

M.K., V.C. and G.R. conceived the idea. G.R. designed the global experiment and developed the Cd isotopes determination with contributions of V.C. and Z.V. (Cd separation and TIMS measurements). R.M. and G.R. performed the modelling and the interpretation. G.R. drafted the manuscript with inputs from all authors with extended participation of D.G., specifically on the ocean discussion part. M.K. was responsible for funding acquisition.

References

1. Rosman, K. J. R. & De Laeter, J. R. The isotopic composition of cadmium in terrestrial minerals. *International Journal of Mass Spectrometry and Ion Physics* **16**, 385–394 (1975).
2. Rosman, K. J. R., De Laeter, J. R. & Gorton, M. P. Cadmium isotope fractionation in fractions of two H3 chondrites. *Earth and Planetary Science Letters* **48**, 166–170 (1980).

3. Ripperger, S., Rehkämper, M., Porcelli, D. & Halliday, A. Cadmium isotope fractionation in seawater—A signature of biological activity. *Earth and Planetary Science Letters* **261**, 670–684 (2007).
4. Abouchami, W. *et al.* Modulation of the Southern Ocean cadmium isotope signature by ocean circulation and primary productivity. *Earth and Planetary Science Letters* **305**, 83–91 (2011).
5. Conway, T. M. & John, S. G. Biogeochemical cycling of cadmium isotopes along a high-resolution section through the North Atlantic Ocean. *Geochimica et Cosmochimica Acta* **148**, 269–283 (2015).
6. Guinoiseau, D. *et al.* Importance of cadmium sulfides for biogeochemical cycling of Cd and its isotopes in Oxygen Deficient Zones–a case study of the Angola Basin. *Global Biogeochemical Cycles* (2019).
7. Wei, R. *et al.* Fractionation of stable cadmium isotopes in the cadmium tolerant Ricinus communis and hyperaccumulator Solanum nigrum. *Scientific reports* **6**, 24309 (2016).
8. Wiggenhauser, M. *et al.* Cadmium isotope fractionation in soil–wheat systems. *Environmental science & technology* **50**, 9223–9231 (2016).
9. Wiggenhauser, M. *et al.* Using isotopes to trace freshly applied cadmium through mineral phosphorus fertilization in soil-fertilizer-plant systems. *Science of the total environment* **648**, 779–786 (2019).
10. Imseng, M. *et al.* Fate of Cd in agricultural soils: A stable isotope approach to anthropogenic impact, soil formation and soil-plant cycling. *Environmental Science & Technology* (2018).
11. Zhou, J.-W. *et al.* Cadmium Isotopic Fractionation in the Soil–Plant System during Repeated Phytoextraction with a Cadmium Hyperaccumulating Plant Species. *Environmental Science & Technology* **54**, 13598–13609 (2020).
12. Cloquet, C., Carignan, J., Libourel, G., Sterckeman, T. & Perdrix, E. Tracing source pollution in soils using cadmium and lead isotopes. *Environmental science & technology* **40**, 2525–2530 (2006).
13. Shiel, A. E., Weis, D. & Orians, K. J. Evaluation of zinc, cadmium and lead isotope fractionation during smelting and refining. *Sci. Total Environ.* **408**, 2357–2368 (2010).

14. Chrastný, V. *et al.* Cadmium isotope fractionation within the soil profile complicates source identification in relation to Pb–Zn mining and smelting processes. *Chemical Geology* **405**, 1–9 (2015).
15. Martinková, E. *et al.* Cadmium isotope fractionation of materials derived from various industrial processes. *Journal of hazardous materials* **302**, 114–119 (2016).
16. Wasylenki, L. E., Swihart, J. W. & Romaniello, S. J. Cadmium isotope fractionation during adsorption to Mn oxyhydroxide at low and high ionic strength. *Geochimica et Cosmochimica Acta* **140**, 212–226 (2014).
17. Horner, T. J., Rickaby, R. E. & Henderson, G. M. Isotopic fractionation of cadmium into calcite. *Earth and Planetary Science Letters* **312**, 243–253 (2011).
18. Guinoiseau, D., Galer, S. J. & Abouchami, W. Effect of cadmium sulphide precipitation on the partitioning of Cd isotopes: Implications for the oceanic Cd cycle. *Earth and Planetary Science Letters* **498**, 300–308 (2018).
19. Xie, X., Yan, L., Li, J., Guan, L. & Chi, Z. Cadmium isotope fractionation during Cd-calcite coprecipitation: Insight from batch experiment. *Science of The Total Environment* 143330 (2020).
20. Järup, L. & Åkesson, A. Current status of cadmium as an environmental health problem. *Toxicology and applied pharmacology* **238**, 201–208 (2009).
21. Järup, L., Berglund, M., Elinder, C. G., Nordberg, G. & Vanter, M. Health effects of cadmium exposure–a review of the literature and a risk estimate. *Scandinavian journal of work, environment & health* 1–51 (1998).
22. Godt, J. *et al.* The toxicity of cadmium and resulting hazards for human health. *Journal of occupational medicine and toxicology* **1**, 22 (2006).
23. Cullen, J. T. & Maldonado, M. T. Biogeochemistry of cadmium and its release to the environment. in *Cadmium: from toxicity to essentiality* 31–62 (Springer, 2013).
24. Nriagu, J. O. Global metal pollution: poisoning the biosphere? *Environment: Science and Policy for Sustainable Development* **32**, 7–33 (1990).

25. Wedepohl, K. H. The composition of the continental crust. *Geochimica et cosmochimica Acta* **59**, 1217–1232 (1995).

26. Rudnick, R. L. & Gao, S. The crust. Treatise on geochemistry. *Elsevier Ltd. Oxford* **3**, 1–64 (2003).

27. Du, H., Peacock, C. L., Chen, W. & Huang, Q. Binding of Cd by ferrihydrite organo-mineral composites: implications for Cd mobility and fate in natural and contaminated environments. *Chemosphere* **207**, 404–412 (2018).

28. Horner, T. J., Lee, R. B., Henderson, G. M. & Rickaby, R. E. Nonspecific uptake and homeostasis drive the oceanic cadmium cycle. *Proceedings of the National Academy of Sciences* **110**, 2500–2505 (2013).

29. Kipton, H., Powell, J. & Town, R. M. Solubility and fractionation of humic acid; effect of pH and ionic medium. *Analytica Chimica Acta* **267**, 47–54 (1992).

30. Stevenson, F. J. *Humus chemistry: genesis, composition, reactions*. (John Wiley & Sons, 1994).

31. Klučáková, M. & Pekař, M. Solubility and dissociation of lignitic humic acids in water suspension. *Colloids and Surfaces A: Physicochemical and Engineering Aspects* **252**, 157–163 (2005).

32. McKnight, D. M. & Aiken, G. R. Sources and age of aquatic humus. in *Aquatic humic substances* 9–39 (Springer, 1998).

33. Yonebayashi, K. & Hattori, T. Chemical and biological studies on environmental humic acids: I. Composition of elemental and functional groups of humic acids. *Soil Science and Plant Nutrition* **34**, 571–584 (1988).

34. Kerndorff, H. & Schnitzer, M. Sorption of metals on humic acid. *Geochimica et Cosmochimica Acta* **44**, 1701–1708 (1980).

35. Tan, K. H. *Environmental soil science.* (Marcel Dekker, Inc., 1994).

36. Pandey, A. K., Pandey, S. D. & Misra, V. Stability constants of metal–humic acid complexes and its role in environmental detoxification. *Ecotoxicology and environmental safety* **47**, 195–200 (2000).

37. Pandey, A. K., Pandey, S. D., Misra, V. & Viswanathan, P. N. Formation of soluble complexes of metals with humic acid and its environmental significance. *Chemistry and Ecology* **16**, 269–282 (1999).

38. Zeledón- Toruño, Z., Lao- Luque, C. & Solé- Sardans, M. Nickel and copper removal from aqueous solution by an immature coal (leonardite): effect of pH, contact time and water hardness. *Journal of Chemical Technology & Biotechnology: International Research in Process, Environmental & Clean Technology* **80**, 649–656 (2005).

39. Lao, C., Zeledón, Z., Gamisans, X. & Solé, M. Sorption of Cd (II) and Pb (II) from aqueous solutions by a low-rank coal (leonardite). *Separation and purification technology* **45**, 79–85 (2005).

40. Chammui, Y., Sooksamiti, P., Naksata, W., Thiansem, S. & Arqueropanyo, O. Removal of arsenic from aqueous solution by adsorption on Leonardite. *Chemical Engineering Journal* **240**, 202–210 (2014).

41. Fowkes, W. W. & Frost, C. M. *Leonardite: a lignite byproduct*. vol. 5611 (US Department of the Interior, Bureau of Mines, 1960).

42. Vermeer, A. W. P., Van Riemsdijk, W. H. & Koopal, L. K. Adsorption of humic acid to mineral particles. 1. Specific and electrostatic interactions. *Langmuir* **14**, 2810–2819 (1998).

43. Marsac, R., Davranche, M., Gruau, G. & Dia, A. Metal loading effect on rare earth element binding to humic acid: Experimental and modelling evidence. *Geochimica et Cosmochimica Acta* **74**, 1749–1761 (2010).

44. Gustafsson, J. P. Visual MINTEQ ver. 3.0. *http://www2. lwr. kth. se/English/OurSoftware/vminteq/index. htm* (2010).

45. Benedetti, M. F. *et al.* Metal ion binding by natural organic matter: from the model to the field. *Geochimica et Cosmochimica Acta* **60**, 2503–2513 (1996).

46. Benedetti, M. F., Milne, C. J., Kinniburgh, D. G., Van Riemsdijk, W. H. & Koopal, L. K. Metal ion binding to humic substances: application of the non-ideal competitive adsorption model. *Environmental Science & Technology* **29**, 446–457 (1995).

47. Koopal, L. K., Saito, T., Pinheiro, J. P. & Van Riemsdijk, W. H. Ion binding to natural organic matter: general considerations and the NICA–Donnan model. *Colloids and Surfaces A: Physicochemical and Engineering Aspects* **265**, 40–54 (2005).

48. Milne, C. J., Kinniburgh, D. G. & Tipping, E. Generic NICA-Donnan model parameters for proton binding by humic substances. *Environmental Science & Technology* **35**, 2049–2059 (2001).

49. Milne, C. J., Kinniburgh, D. G., Van Riemsdijk, W. H. & Tipping, E. Generic NICA− Donnan model parameters for metal-ion binding by humic substances. *Environmental Science & Technology* **37**, 958–971 (2003).

50. Schmitt, A.-D., Galer, S. J. & Abouchami, W. Mass-dependent cadmium isotopic variations in nature with emphasis on the marine environment. *Earth and Planetary Science Letters* **277**, 262–272 (2009).

51. Schmitt, A.-D., Galer, S. J. & Abouchami, W. High-precision cadmium stable isotope measurements by double spike thermal ionisation mass spectrometry. *Journal of Analytical Atomic Spectrometry* **24**, 1079–1088 (2009).

52. Abouchami, W. *et al.* Biogeochemical cycling of cadmium isotopes in the Southern Ocean along the Zero Meridian. *Geochimica et Cosmochimica Acta* **127**, 348–367 (2014).

53. Abouchami, W. *et al.* A common reference material for cadmium isotope studies–NIST SRM 3108. *Geostandards and Geoanalytical Research* **37**, 5–17 (2013).

54. Li, D., Li, M.-L., Liu, W.-R., Qin, Z.-Z. & Liu, S.-A. Cadmium isotope ratios of standard solutions and geological reference materials measured by MC- ICP- MS. *Geostandards and Geoanalytical Research* **42**, 593–605 (2018).

55. Liu, M.-S. *et al.* High- Precision Cd Isotope Measurements of Soil and Rock Reference Materials by MC- ICP- MS with Double Spike Correction. *Geostandards and Geoanalytical Research* **44**, 169–182 (2020).

56. Tan, D. *et al.* High-sensitivity determination of Cd isotopes in low-Cd geological samples by double spike MC-ICP-MS. *Journal of Analytical Atomic Spectrometry* **35**, 713–727 (2020).

57. Ravel, B. & Newville, M. ATHENA, ARTEMIS, HEPHAESTUS: data analysis for X-ray absorption spectroscopy using IFEFFIT. *Journal of synchrotron radiation* **12**, 537–541 (2005).

58. Harrison, W. & Trotter, J. Crystal and molecular structure of cadmium diacetate dihydrate. *Journal of the Chemical Society, Dalton Transactions* 956–960 (1972).

59. Kinniburgh, D. G. *et al.* Ion binding to natural organic matter: competition, heterogeneity, stoichiometry and thermodynamic consistency. *Colloids and Surfaces A: Physicochemical and Engineering Aspects* **151**, 147–166 (1999).

60. Kinniburgh, D. G. *et al.* Metal ion binding by humic acid: application of the NICA-Donnan model. *Environmental Science & Technology* **30**, 1687–1698 (1996).

61. Meng, F., Yuan, G., Wei, J., Bi, D. & Wang, H. Leonardite-derived humic substances are great adsorbents for cadmium. *Environmental Science and Pollution Research* **24**, 23006–23014 (2017).

62. Liu, C., Frenkel, A. I., Vairavamurthy, A. & Huang, P. M. Sorption of cadmium on humic acid: Mechanistic and kinetic studies with atomic force microscopy and X-ray absorption fine structure spectroscopy. *Canadian Journal of Soil Science* **81**, 337–348 (2001).

63. de Melo, B. A. G., Motta, F. L. & Santana, M. H. A. Humic acids: Structural properties and multiple functionalities for novel technological developments. *Materials Science and Engineering: C* **62**, 967–974 (2016).

64. Von Wandruszka, R., Ragle, C. & Engebretson, R. The role of selected cations in the formation of pseudomicelles in aqueous humic acid. *Talanta* **44**, 805–809 (1997).

65. Avena, M. J., Vermeer, A. W. P. & Koopal, L. K. Volume and structure of humic acids studied by viscometry: pH and electrolyte concentration effects. *Colloids and Surfaces A: Physicochemical and Engineering Aspects* **151**, 213–224 (1999).

66. Tombácz, E. Colloidal properties of humic acids and spontaneous changes of their colloidal state under variable solution conditions. *Soil Science* **164**, 814–824 (1999).

667 67. Dideriksen, K., Baker, J. A. & Stipp, S. L. S. Equilibrium Fe isotope fractionation between inorganic
668 aqueous Fe (III) and the siderophore complex, Fe (III)-desferrioxamine B. *Earth and Planetary*
669 *Science Letters* **269**, 280–290 (2008).
670 68. Jouvin, D., Louvat, P., Juillot, F., Maréchal, C. N. & Benedetti, M. F. Zinc isotopic fractionation:
671 why organic matters. *Environmental science & technology* **43**, 5747–5754 (2009).
672 69. Bigalke, M., Weyer, S. & Wilcke, W. Copper isotope fractionation during complexation with
673 insolubilized humic acid. *Environmental science & technology* **44**, 5496–5502 (2010).
674 70. Ryan, B. M., Kirby, J. K., Degryse, F., Scheiderich, K. & McLaughlin, M. J. Copper isotope
675 fractionation during equilibration with natural and synthetic ligands. *Environmental science &*
676 *technology* **48**, 8620–8626 (2014).
677 71. Juillot, F. *et al.* Zn isotopic fractionation caused by sorption on goethite and 2-Lines ferrihydrite.
678 *Geochimica et Cosmochimica Acta* **72**, 4886–4900 (2008).
679 72. Guinoiseau, D., Gélabert, A., Moureau, J., Louvat, P. & Benedetti, M. F. Zn isotope fractionation
680 during sorption onto kaolinite. *Environmental science & technology* **50**, 1844–1852 (2016).
681 73. Bigeleisen, J. & Mayer, M. G. Calculation of equilibrium constants for isotopic exchange reactions.
682 *The Journal of Chemical Physics* **15**, 261–267 (1947).
683 74. Schauble, E. A. Applying stable isotope fractionation theory to new systems. *Reviews in Mineralogy*
684 *and Geochemistry* **55**, 65–111 (2004).
685 75. Yang, J. *et al.* Theoretical calculations of Cd isotope fractionation in hydrothermal fluids. *Chemical*
686 *Geology* **391**, 74–82 (2015).
687 76. Ohtaki, H. & Johansson, G. X-ray diffraction studies on the structures of cadmium iodide complexes
688 in water and in DMSO solutions. *Pure and Applied Chemistry* **53**, 1357–1364 (1981).
689 77. Mohammed, A. M. Hydration of Cd (II): molecular dynamics study. *Bulletin of the Chemical*
690 *Society of Ethiopia* **22**, (2008).

78. Boyanov, M. I. *et al.* Adsorption of cadmium to Bacillus subtilis bacterial cell walls: a pH-dependent X-ray absorption fine structure spectroscopy study. *Geochimica et Cosmochimica Acta* **67**, 3299–3311 (2003).

79. Vasconcelos, I. F., Haack, E. A., Maurice, P. A. & Bunker, B. A. EXAFS analysis of cadmium (II) adsorption to kaolinite. *Chemical Geology* **249**, 237–249 (2008).

80. Bazarkina, E. F., Pokrovski, G. S., Zotov, A. V. & Hazemann, J.-L. Structure and stability of cadmium chloride complexes in hydrothermal fluids. *Chemical Geology* **276**, 1–17 (2010).

81. Wiggenhauser, M. *et al.* Cadmium transfer in contaminated soil-rice systems: Insights from solid-state speciation analysis and stable isotope fractionation. *Environmental Pollution* **269**, 115934 (2021).

82. Gondar, D., López, R., Fiol, S., Antelo, J. M. & Arce, F. Cadmium, lead, and copper binding to humic acid and fulvic acid extracted from an ombrotrophic peat bog. *Geoderma* **135**, 196–203 (2006).

83. Carrasquero-Durán, A. & Flores, I. Cadmium Binding by Humic Acids: An Experiment in FTIR Spectroscopy and Soil Chemistry. *Chem. Educ.* **9**, 1–4 (2004).

84. Karlsson, T., Persson, P. & Skyllberg, U. Extended X-ray absorption fine structure spectroscopy evidence for the complexation of cadmium by reduced sulfur groups in natural organic matter. *Environmental science & technology* **39**, 3048–3055 (2005).

85. Isaure, M.-P. *et al.* Evidence of various mechanisms of Cd sequestration in the hyperaccumulator Arabidopsis halleri, the non-accumulator Arabidopsis lyrata, and their progenies by combined synchrotron-based techniques. *Journal of experimental botany* **66**, 3201–3214 (2015).

86. Imseng, M. *et al.* Towards an understanding of the Cd isotope fractionation during transfer from the soil to the cereal grain. *Environmental pollution* **244**, 834–844 (2019).

87. Huggins, M. L. Bond energies and polarities1. *Journal of the American Chemical Society* **75**, 4123–4126 (1953).

88. Hiemstra, T. & Van Riemsdijk, W. H. On the relationship between charge distribution, surface hydration, and the structure of the interface of metal hydroxides. *Journal of colloid and interface science* **301**, 1–18 (2006).

89. Carbonaro, R. F. & Di Toro, D. M. Linear free energy relationships for metal–ligand complexation: monodentate binding to negatively-charged oxygen donor atoms. *Geochimica et cosmochimica acta* **71**, 3958–3968 (2007).

90. Wilkins, R. G. Mechanisms of ligand replacement in octahedral nickel (II) complexes. *Accounts of Chemical Research* **3**, 408–416 (1970).

91. Elias, H. R. G. Wilkins: Kinetics and Mechanism of Reactions of Transition Metal Complexes, 2nd Thoroughly Revised Edition. VCH, Weinheim 1991. ISBN 3–527–28389–7. 482 Seiten. Preis (Softcover): DM 68.00. *Berichte der Bunsengesellschaft für physikalische Chemie* **96**, 638–639 (1992).

92. Chillemi, G. *et al.* Computational evidence for a variable first shell coordination of the cadmium (II) ion in aqueous solution. *The Journal of Physical Chemistry B* **109**, 9186–9193 (2005).

93. Pye, C. C., Tomney, M. R. & Rudolph, W. W. Cadmium hydration: hexacoordinate or heptacoordinate? *Canadian Journal of Analytical Sciences and Spectroscopy* **51**, 140–146 (2006).

94. D'Angelo, P., Migliorati, V., Mancini, G. & Chillemi, G. A coupled molecular dynamics and XANES data analysis investigation of aqueous cadmium (II). *The Journal of Physical Chemistry A* **112**, 11833–11841 (2008).

95. Saito, T., Nagasaki, S., Tanaka, S. & Koopal, L. K. Electrostatic interaction models for ion binding to humic substances. *Colloids and Surfaces A: Physicochemical and Engineering Aspects* **265**, 104–113 (2005).

96. Mendoza-Cózatl, D. G., Jobe, T. O., Hauser, F. & Schroeder, J. I. Long-distance transport, vacuolar sequestration, tolerance, and transcriptional responses induced by cadmium and arsenic. *Current opinion in plant biology* **14**, 554–562 (2011).

97. Vogel-Mikuš, K., Arčon, I. & Kodre, A. Complexation of cadmium in seeds and vegetative tissues of the cadmium hyperaccumulator Thlaspi praecox as studied by X-ray absorption spectroscopy. *Plant and Soil* **331**, 439–451 (2010).

98. Huguet, S. *et al.* Cd speciation and localization in the hyperaccumulator Arabidopsis halleri. *Environmental and Experimental Botany* **82**, 54–65 (2012).

99. Ueno, D., Ma, J. F., Iwashita, T., Zhao, F.-J. & McGrath, S. P. Identification of the form of Cd in the leaves of a superior Cd-accumulating ecotype of Thlaspi caerulescens using 113 Cd-NMR. *Planta* **221**, 928–936 (2005).

100. Tian, S. *et al.* Cellular sequestration of cadmium in the hyperaccumulator plant species Sedum alfredii. *Plant Physiology* **157**, 1914–1925 (2011).

101. Xue, Z. *et al.* Cadmium isotope variations in the Southern Ocean. *Earth and Planetary Science Letters* **382**, 161–172 (2013).

102. Xie, R. C. *et al.* Non-Rayleigh control of upper-ocean Cd isotope fractionation in the western South Atlantic. *Earth and planetary science letters* **471**, 94–103 (2017).

103. Bruland, K. W. Complexation of cadmium by natural organic ligands in the central North Pacific. *Limnology and Oceanography* **37**, 1008–1017 (1992).

104. Ellwood, M. J. Zinc and cadmium speciation in subantarctic waters east of New Zealand. *Marine Chemistry* **87**, 37–58 (2004).

105. Baars, O., Abouchami, W., Galer, S. J., Boye, M. & Croot, P. L. Dissolved cadmium in the Southern Ocean: Distribution, speciation, and relation to phosphate. *Limnology and Oceanography* **59**, 385–399 (2014).

106. Louis, Y. *et al.* Characterisation and modelling of marine dissolved organic matter interactions with major and trace cations. *Marine Environmental Research* **67**, 100–107 (2009).

107. Pokrovsky, O. S., Pokrovski, G. S., Gélabert, A., Schott, J. & Boudou, A. Speciation of Zn associated with diatoms using X-ray absorption spectroscopy. *Environmental science & technology* **39**, 4490–4498 (2005).

108. Gélabert, A. *et al.* Interaction between zinc and freshwater and marine diatom species: surface complexation and Zn isotope fractionation. *Geochimica et Cosmochimica Acta* **70**, 839–857 (2006).
109. Sieber, M. *et al.* Physical and biogeochemical controls on the distribution of dissolved cadmium and its isotopes in the Southwest Pacific Ocean. *Chemical Geology* **511**, 494–509 (2019).